Pramana – J. Phys. (2016) 87: 9
DOI 10.1007/s12043-016-1212-z

Shock wave propagation in soda lime glass using optical shadowgraphy

Y B S R PRASAD[1,2,*], S BARNWAL[1,2], P A NAIK[1,2], Y YADAV[3], R PATIDAR[1,2], M P KAMATH[1], A UPADHYAY[1,2], S BAGCHI[1], A KUMAR[1], A S JOSHI[1] and P D GUPTA[1,2]

[1]Laser Plasma Division, Raja Ramanna Centre for Advanced Technology, Indore 452 013, India
[2]Homi Bhabha National Institute, Anushaktinagar, Mumbai 400 094, India
[3]School of Physics, DAVV Indore, Indore 452 001, India
*Corresponding author. E-mail: yprasad@rrcat.gov.in

MS received 11 June 2015; accepted 21 August 2015; published online 16 June 2016

Abstract. Propagation of shock waves in soda lime glass, which is a transparent material, has been studied using the optical shadowgraphy technique. The time-resolved shock velocity information has been obtained (1) in single shot, using the chirped pulse shadowgraphy technique, with a temporal resolution of tens of picoseconds and (2) in multiple shots, using conventional snapshot approach, with a second harmonic probe pulse. Transient shock velocities of (5–7) $\times$ 10^6 cm/s have been obtained. The scaling of the shock velocity with intensity in the 2×10^{13}–10^{14} W/cm^2 range has been obtained. The shock velocity is observed to scale with laser intensity as $I^{0.38}$. The present experiments also show the presence of ionization tracks, generated probably due to X-ray hotspots from small-scale filamentation instabilities. The results and various issues involved in these experiments are discussed.

Keywords. Shock velocity; soda lime glass; chirped pulse shadowgraphy.

PACS Nos 52.50.Jm; 52.50.Lp; 52.70.Kz

1. Introduction

Dynamic pressures of several hundreds of megabars are generated when samples are irradiated with intense laser beams. The interest to study how different materials respond to the propagation of these strong shock waves originates from the applications in the fields of inertial confinement fusion, astrophysics, and geophysics [1–3]. Earlier on, diamond anvil cells (static pressures) [4], light guns [5,6] etc. were used to generate high-pressure conditions in different materials. These pressures are much lower than the pressures from laser-produced plasmas. With the advent of high-power laser systems delivering several hundreds of kilojoules of energy, this transient pressure range is extended from several hundreds of megabars to gigabars [7–9] through intense shock wave generation for laser intensities of 10^{13-15} W/cm^2. As these pressures are dynamic in nature, being generated by intense shock waves generated due to strong recoil by the expanding laser-produced plasma, it is interesting to study how these shocks evolve in space and time. As shock waves travel in the medium at very high velocities, they create a near discontinuity in material properties like pressure, temperature, and density across the shock front. These material properties, before and after the shock wave propagation, are related to each other through the well-known Rankine–Hugoniot equations [10].

$$\rho_0 U_\mathrm{s} = \rho_1 (U_\mathrm{s} - U_\mathrm{p}), \tag{1}$$

$$P_1 - P_0 = \rho_0 U_\mathrm{s} U_\mathrm{p}, \tag{2}$$

$$E_1 - E_0 = 0.5(P_1 + P_0)(1/\rho_0 - 1/\rho_1), \tag{3}$$

where ρ_0, P_0, E_0, ρ_1, P_1, E_1 refer to the mass density, pressure and internal energy of the undisturbed (i.e. before the passage of shock wave) material, and the shocked material, respectively. U_s and U_p are the shock and particle velocities. These three relations represent the conservation of mass, momentum, and energy before and after the shock. In order to measure these material properties, any two parameters need to be experimentally measured independently. Usually,

the shock wave velocity and the particle velocity are the two parameters measured using different experimental techniques. As the velocity of the shock wave is proportional to the amplitude of the wave, for a laser pulse, the shock wave velocity increases in the rising part of the laser pulse, leading to coalescing [11] of the shock waves. Similarly, once the laser pulse is over, the compressed material starts relaxing and thus a rarefaction wave propagates in the medium with a velocity which is more than that of the shock wave preceding it. Eventually, the rarefaction wave overtakes the preceding shock front and weakens it. As these experiments are carried out in thin (few micron thick) material foils, the time-scales are typically a few nanoseconds. Hence, fast detectors like optical streak cameras [12] or external laser probes of short duration are used to study the time evolution. However, as a streak camera detects the optical luminosity signal which is generated only when shock reaches the rear side of the foil, it gives the time-averaged shock velocity.

It is possible to study temporal evolution of the shock waves using an external optical probe passing through the irradiated region. To study evolution of the shock speed using this technique, one requires the material to be transparent to the probing radiation. Different techniques like (a) velocity interferometer system for any reflector (VISAR) [13], (b) passing a long-duration probe beam in the transverse direction coupled with an optical streak camera [14], (c) multiple snapshot approach [15] using a short-duration probe etc., are used for this purpose. The VISAR can be used to study the propagation of a moving shock front by illuminating from the rear side of a transparent target and recording the variation in fringe-shift with time. As the shock front propagates, the shocked material gets ionized and the shock front acts as good transient reflector for the probing radiation. However, the VISAR technique has a limit on the time resolution of several tens of picoseconds. Similarly, a long-duration probe can be sent tangentially to the shocked region of the target and the resultant propagation of the shadow region caused by the propagating shock wave can be recorded using a streak camera to calculate the shock velocity and its variation in time. However, this technique requires a synchronized long-duration probe pulse and here also the temporal resolution is limited by the streak camera. The advent of chirped pulse amplification (CPA) [16] based lasers has opened up a simpler alternative to probe the evolution of shock wave propagation in a single shot. In the CPA technique, the fs laser pulse from the oscillator is stretched in time to several hundreds of picoseconds by spectrally dispersing the laser pulse in time (i.e., frequency chirped). This low intensity pulse is then amplified further and compressed back in time to get an ultraintense fs pulse. The stretched chirped pulse is useful for probing as its spectrum carries the time information.

The optical shadowgraphy experiments were carried out at the Raja Ramanna Centre for Advanced Technology, Indore, India, using the chirped pulse shadowgraphy technique as well as the snap-shot technique, to study the evolution of shock waves in transparent soda lime glass targets and to observe the temporal variation of the shock velocity. A high power Nd:glass laser system [17] was used in these experiments. To the best of our knowledge, this is the first time that chirped shadowgraphy was used to study the dynamics of shock wave propagation in a transparent medium. The measured shock velocities indicate a transient behaviour with time that can be associated with non-equilibrium. The results from the experiments are presented in this paper.

Hugoniot information of the transparent soda lime (commercial microscope slides) glass, at different laser intensities between 10^{13} and 10^{14} W/cm^2 has also been obtained. The intensity scaling has been obtained as $I^{0.38}$. In addition, the present experiments also show the formation of jet-like ionization channels in the glass target behind the front edge in time-resolved shadowgrams. The time-integrated pictures also reveal a tree-like structure which, in literature, has been attributed to the internal electrical breakdown occurring in the glass material due to high electrical fields (10^8 V/m) near 'charged' laser-produced plasmas [24]. The details of the experiment and the results are discussed here.

2. Experimental set-up

2.1 *Chirped pulse shadowgraphy*

Experiments were carried out using an Nd:phosphate glass high power laser system [17]. In this laser system, a 100 fs oscillator pulse at 1054 nm (Coherent : Chameleon) was stretched in a grating-based pulse stretcher to 650 ps (FWHM) and amplified in a regenerative amplifier to a few mJ level (gain of 10^7) [18]. This pulse was then amplified in an amplifier chain to an energy up to 10 J. The heating beam was focussed using a doublet lens ($f = 50$ cm) providing a large depth of focus, to a focal spot of $\sim$100 μm, leading to laser intensities of 10^{13-14} W/cm^2. A schematic diagram of the experimental set-up is shown in figure 1. The targets were commercially available

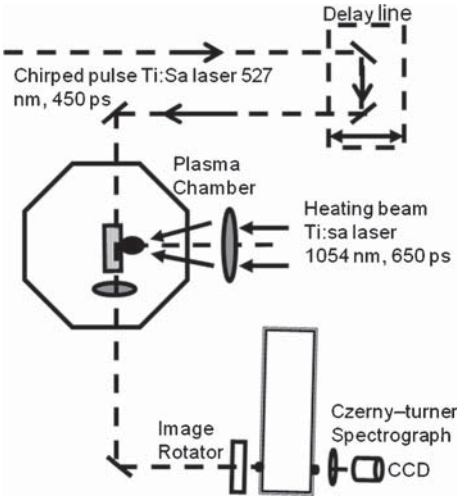

Figure 1. A schematic diagram of the experimental set-up.

microscope glass slides (1.3 mm × 25 mm × 75 mm) made of soda lime glass [typically SiO_2(73.2), Na_2O (10.6), CaO(9.4), MgO(3.1), $A1_2O_3$(1.8), K_2O(1.1), TiO_2(0.6), Fe_2O_3(0.2), but varies across the samples] [19]. The central part of the thin side of the glass slide (1.3 mm) was irradiated with laser pulses. They were mounted on a target movement system placed in a vacuum chamber, to expose fresh target surface after each shot.

In order to study temporal evolution of shock wave propagation in the transparent sample, a synchronized probe pulse with well-defined chirp was required. For this purpose, a portion of the stretched laser pulse (650 ps) was split using a beam splitter after the fifth amplifier stage in the system. In some shots, this pulse was converted into its second harmonic using a KDP crystal (450 ps duration). The bandwidth of the probe beam after passing through the laser chain was ∼2.5 nm. This probe beam was passed through a set of relays and a delay line, and then made to pass through the target tangentially. The relays were used to relay the probe beam over several metres to minimize spatial distortions. Secondly, they also provided the necessary demagnification of the probe beam (from 40 mm to 15 mm). A variable delay line was used first to synchronize the probe beam with the heating beam to an accuracy of 100 ps (measured using a fast photodiode) and then to introduce known delays. A He–Ne laser beam collinear with this probe was used for aligning the optical elements.

In order to get a higher spatial resolution, a small region of the plasma plane was imaged onto the 50 μm wide entrance slit of a Czerny–Turner spectrograph (Digikrom 480 from CVI) with a large magnification of ∼40×–60×. The spectrograph had a grating of 1200 grooves/mm to disperse the probe beam with a spectral resolution of 0.3 nm. The image was rotated by 90° with the help of an image rotator (based on prisms) placed just before the entrance slit, as it was necessary to have the shock wave (and thus shadow) propagation parallel to the direction of spectral dispersion to avoid smearing of information. The spectral output at the exit plane of the spectrograph (exit slit removed) was imaged using a charge coupled device (CCD) camera with suitable demagnification. Thus, in the recorded images, the horizontal axis (direction of spectral dispersion) provides the temporal information, whereas the vertical direction gives the spatial information of the shock wave (shadow) movement.

2.2 *Snap-shot shadowgraphy*

In order to obtain time-resolved shock velocity information independently, shadowgraphy experiments were also conducted using conventional snap-shot approach. For this purpose, the laser pulses from a commercial laser oscillator (EKSPLA, SBS pulse compression) delivering 500 ps (FWHM) pulses at 1054 nm wavelength were later amplified to 1–10 J energy in the amplifier chain of the high power laser system. In this case also, a part of the laser beam was converted to its second harmonic using a KDP crystal, to probe the shock wave propagation. The experimental set-up used in this experiment was similar to that shown in figure 1, except that the spectrograph was replaced by a simple CCD camera. The probe beam was incident on the target tangentially. The image magnification was nearly the same in this set-up also. As a large-area detector was needed, a DSLR camera (Canon 550 D – 22.5 × 15 mm^2, 4.3 μm/pixel) was used in the experiment. Interference filters for 527 nm ($\Delta\lambda \sim \pm 10$ nm) were placed before the detector to block all other wavelengths (plasma luminosity) other than the probe laser. These were in addition to the neutral density filters which were used to reduce the recorded shadowgrams below the saturation level of the CCD pixels.

A major hurdle in recording the shock propagation in the early delay times (i.e., up to 1 ns) is the shadow of the target front edge itself. Unless the target surface is flat and kept perfectly tangential to the probe beam, a finite shadow is seen due to the projection of the front surface. To reduce this, a precise target rotator was used. Moreover, use of back reflection from the glass target surface ensured that the target is exactly perpendicular to the heating/probing laser beams.

3. Results and discussion

3.1 *Results from chirped pulsed shadowgraphy*

A typical shadowgram with the probe beam passing through the shocked regions is shown in figure 2a. A reference shadowgram was also taken in the absence of the heating beam, which is shown in figure 2b. The propagation of shock wave through the transparent material leads to an increase in material density (compression) and the resultant sharp change in refractive index of the material causes the formation of a shadow. In conventional shadowgraphy experiments, the shock velocity is calculated from the extent of this shadow region at different instances of time. However, in the case of chirped shadowgraphy experiments, as the wavelength of the probe beam varies at a definite rate (chirp), different instances of the propagating shadow get imaged at different positions on the spectrum. Thus, the transmitted spectrum gives a continuous time history of the propagating shock wave. As the probe beam in our case had a linear positive chirp (i.e., longer wavelengths appearing earlier in time), these images show temporal evolution from the right side to the left side. Using the known chirp factor of the probe pulse (650 ps/2.5 nm) and the known dispersion factor of the spectrograph, the recorded spectrum corresponds to ∼450 ps. The velocity of the moving shadow can be obtained from the slope of the interface between the opaque (dark) and bright regions in figure 2a. As one tracks along the slope at different points of time, one gets the shock velocity profile. A typical temporal

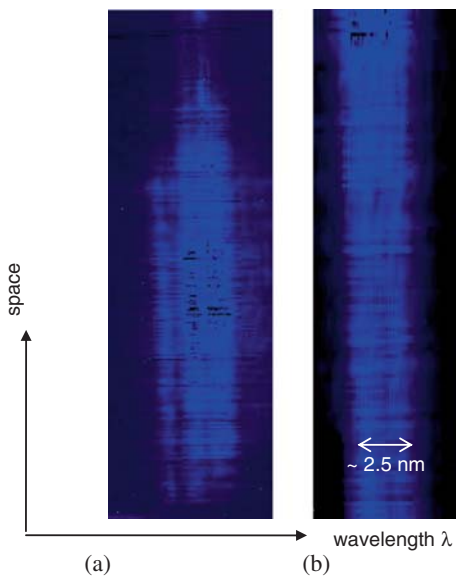

Figure 2. Typical shadowgram (**a**) with and (**b**) without shock wave propagation. Shock is propagating downwards.

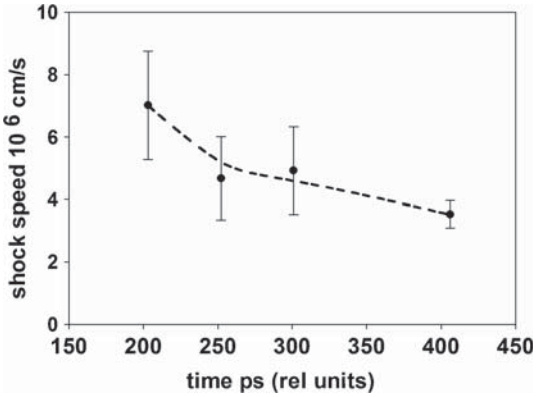

Figure 3. Variation of shock velocity with time at $I_L \sim 1 \times 10^{14}$ W/cm^2.

profile of the shock velocity, calculated from the shock front propagation, is shown in figure 3. A peak shock velocity of 7×10^6 cm/s was obtained from the recorded spectrum. The error bars are due to the finite width of the entrance slit (50 μm) of the spectrograph which translates into a $\pm$13 ps error in the temporal calculations, and the same is also reflected in the calculations of shock velocity. This shadowgram was recorded at a laser intensity of $\sim 10^{14}$ W/cm^2.

3.2 *Results from snap-shot shadowgraphy*

A reference shadowgram, recorded in the absence of plasma, is shown in figure 4a. Figure 4b shows a typical shadowgram with the probe beam passing through the shocked region in the target. As the shock wave propagates through the medium, the medium becomes opaque to the probe beam in the shocked region. Hence, the movement of the shadow region represents the movement of the shock front at different instances of time. The temporal profile of the shock velocity was obtained by taking the shadowgrams at different time delays (1–4 ns), and measuring the movement of shock front at different times. Figure 5 shows the shock velocity profile obtained from experimental data at a laser intensity of 10^{14} W/cm^2. The temporal profile of the shock velocity obtained from another set of data taken at a slightly lower intensity of 4×10^{13} W/cm^2, is also shown in the same figure. The error bars on the shock velocity originate from the uncertainty in locating the front surface due to the finite size of its shadow region in the reference image. Hence the error bars are larger for lower time.

3.3 *About the shock wave velocity evolution*

As mentioned in the Introduction, the shock velocity is proportional to the amplitude of the shock wave. For

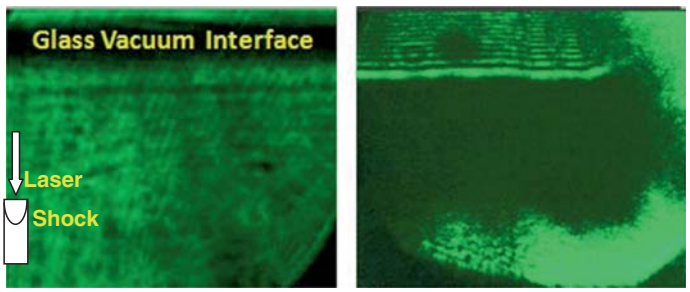

(a) (b)

Figure 4. Typical shadowgram (**a**) without shock and (**b**) with shock wave propagation.

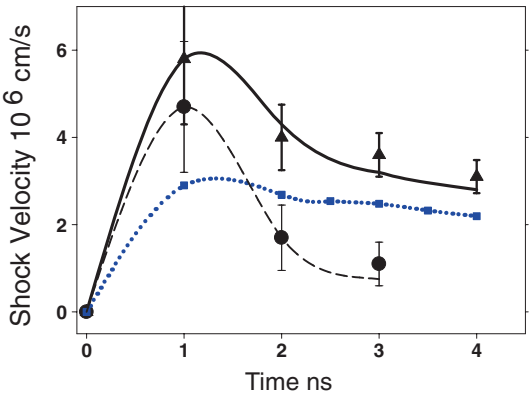

Figure 5. Variation of the shock velocity with time at two laser intensities: 4×10^{13} (filled circles, dashed curve) and 10^{14} W/cm^2 (triangles, solid curve). The curves are only to guide the eyes. Also shown is the simulated velocity profile using MULTI code (squares, dotted curve) for 10^{14} W/cm^2.

a typical laser pulse with a Gaussian temporal profile, the rising portion of the laser pulse can be assumed to be a sequence of short pulses with increasing intensity. This generates a sequence of shock waves of increasing amplitude and hence increasing velocity. As a result, all these shock waves will join each other (i.e., shock coalescence), forming an intense shock front. In the growing phase of the shock wave, shock coalescence will occur for different laser intensities at different times, at different distances from the surface of the target front. Similarly, once the laser pulse is over, the plasma ablation will stop, and in the absence of the compressive drive, the compressed target material will start decompressing, resulting in a rarefaction wave propagating into the compressed material. As the rarefaction wave propagates in the compressed material, as against the shock wave which travels in an uncompressed material, the velocity of the rarefaction wave is more than that of the shock wave, and it eventually overtakes the shock front. Once the rarefaction wave reaches the shock front, the amplitude of the shock wave drops, leading to a fall in the shock velocity (i.e. the 'falling phase' of the shock wave). The distances and times when these two phases will appear and how long they will last, will depend upon (a) laser pulse duration, (b) target material, and finally (c) laser intensity. Rapidly falling shock velocity is seen in figure 3, because in this case, the chirped probe beam was passing through the shocked region 1 ns after the peak of the heating beam.

In order to compare the experimental results with the theory, the propagation of the shock wave in soda lime glass was also simulated using the hydrodynamic code MULTI [20]. The simulations were carried out at a focussed laser intensity of 10^{14} W/cm^2. For these calculations, a mass density of 2.5 g/cm^3 was taken for the glass target. The code provides spatial profile of parameters like mass density and pressure, at different times after the laser pulse is incident on the target. As the shock wave propagates inwards in the target, the height and the width of the density profile changes. The shock velocity was calculated from the location of the shock front (front edge of the density profile) at different times. The simulation results are also shown in figure 5, along with the experimental results. It can be seen that compared to the experimental values, the simulated values are smaller than the experimental values by a factor of 2. However, the trend matches with the experimental observations.

We now have a look at some of the experimental intricacies. As the shocked region propagates only few μm to tens of μm during the duration of the probe beam (for example, a shock wave with 2×10^6 cm/s velocity covers a distance of 10 μm during 500 ps), one needs to have a higher magnification to obtain the shock front movement and thus the velocity variation with good accuracy. However, higher magnification also means that a very small region at the target plane is being imaged on to the entrance slit (length) of the spectrograph. The shock profile can be obtained only if the shock front remains within this region during the duration of the probe beam for the delay set between the two beams (heating and probing). However, if the

energy of the heating beam drastically changes from shot to shot, the shock wave propagation time will change and it will be out of the observation window. Thus, the energy stability is a crucial issue in these experiments.

The single-shot temporal window can be adjusted by varying the stretcher separation or by employing a secondary stretcher for the probe beam to stretch to cover a large time period to obtain complete shock wave propagation, albeit with lesser time resolution. The main advantages of the chirped pulse probe are: (1) single-shot recording of the time variation of the shock speed and (2) the fact that one does not require the knowledge about origin of the shock wave propagation (i.e., target front surface) as the shock wave velocity is calculated from the relative movement of the shock front at different instances of time during the probe beam duration. The temporal resolution and the time period can be adjusted by changing chirp parameters and can either obtain faster time resolution (than possible with the techniques discussed above) in a short temporal window or with a lower time resolution, covering the entire shock evolution.

It should also be noted that as delays used were discrete (1–4 ns) and the peaks occurred around 1 ns, in reality, they could be anywhere between 0.5 and 1.5 ns. To perform shadowgraphy experiments below 1 ns, one needs to overcome the issues associated with the shadow region of the target front surface, mentioned earlier.

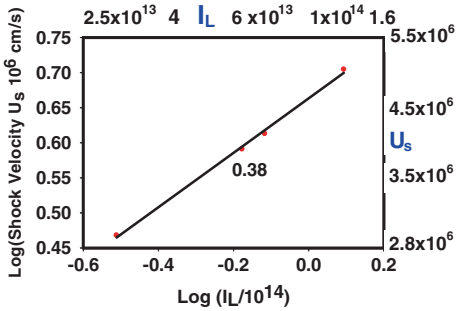

Figure 6. The scaling of the shock velocity and the shock pressure with laser intensity.

3.4 *Intensity scaling of shock velocity*

The shock velocities calculated from these experiments for different laser intensities are shown in figure 6 for a delay of 3 ns. The shock wave velocity ranges from 2.6×10^6 to 4.4×10^6 cm/s for laser intensities from 3×10^{13} to 1.3×10^{14} W/cm^2. The corresponding particle velocity at each point can be calculated using the relation between the shock velocity and the particle velocity in soda lime glass given by Kobayashi *et al* as [21]

$$U_s = 0.14 + 1.92U_p. \quad (4)$$

The particle velocities for the above shock velocities are 1.7×10^6–2.9×10^6 cm/s. Once U_s and U_p are known, the shock pressure can be calculated using the expression $P = \rho_0 U_s U_p$, where ρ_0 is the mass density of the target before the shock. The corresponding shock pressures calculated from these experiments are 8–25 Mbar. It should be noted that the shadow has some non-uniform features as can be seen from figure 4b. This is mainly due to the non-uniform illumination in the laser focal spot region. The velocities and the pressures calculated here are for the maximum shadow position. The scaling of the shock velocity with laser intensity is given in figure 6. The shock velocity (U_s) scales with laser intensity (I_L) as $I_L^{0.38}$.

3.5 *Detection of ionization tracks*

In addition to the shock wave propagation, some other interesting observations were made in these

Table 1. Experimental parameters for figures 7a–7g.

Sl. No.	Image ref.	Laser energy	Intensity (W/cm^2)	Magnification	Probe delay	Penetration depth remarks
1	Img69	2.2 J	5.3×10^{13}	34	2 ns	~135 μm
2	Img70	–	–	34	2 ns	As a reference in the absence of plasma
3	Img74	1.2 J	3×10^{13}	34	Integrated	With He–Ne laser after the shot
4	Img87	–	–	34	Integrated	Another time integrated with He–Ne
5	Img239	5.4	1.4×10^{14}	26	1 ns	~500 μm
6	Img240	5.7	1.5×10^{14}	26	1 ns	To show shift in the diffraction fringes, and the diverging trend in the structures
7	Img230	–	–	26	1 ns	As a reference in the absence of plasma

experiments. With proper imaging and lower magnifications (20–30×), long structures like jet streams were recorded in the target region at different delays. The experimental conditions under which these shadowgrams were recorded are in given in table 1. The shadowgrams recorded after a delay of 2 ns at lower intensities show the presence of ∼130–150 μm long structures (figure 7a). When probed at a delay of 1 ns, for 10^{14} W/cm^2, these structures were ∼500 μm long (figures 7e, 7f). In addition, the time-integrated shadowgrams also showed a tree-like structure centred around the laser focal spot region (figures 7c, 7d). The possible explanation is given below.

First, let us examine the generation of tree-like structures seen in figures 7c, 7d. Fedosejevs *et al* [22] reported similar tree-like structures in plexiglass, behind the irradiated area, extending up to 500 μm, at an intensity of 3×10^{15} W/cm^2, at an optical delay of 0.75 ns and also well after the shot. At lower intensities (10^{14} W/cm^2), the extent of these structures was reduced to ∼60–70 μm at 0.75 ns, which later spread in space with time. They had attributed these well-spread tree-like structures to internal breakdown of the plexiglass due to the intense electrical fields (10^8 V/m) generated close to the positively charged laser-produced plasma. Earlier to this, the presence of huge electrical potential (187 kV) was first reported by Benjamin *et al* [23]. For laser intensities around 10^{14} W/cm^2, Borowitz *et al* had measured the potential in plasmas around 60 kV [24] from Pockels cell measurements. For typical plasma dimensions (R) of $\sim 10^{-4}$ m (∼100 μm), this translates into $\sim 6 \times 10^8$ V/cm, higher than the breakdown fields for silica ($E_b \sim 10^8$ V/cm) [25], corroborating that similar breakdown may be occurring in soda lime glass, leading to structures similar to those observed in the time-integrated shadowgrams seen in figures 7c and 7d.

Now, we discuss the possible origin of the long tracks. It is experimentally seen that for a laser intensity of 5×10^{13} W/cm^2, these structures are ∼130–150 μm long and for 1.5×10^{14} W/cm^2, their length increases to 500 μm. In both the cases, these channels are ∼10 μm wide. We can rule out the presence of electron jets [26], as our intensities are way below to those required to produce hot electrons. It is occasionally seen that in high-energy, long-duration laser systems, hot spots are present in the laser spatial profile leading to the onset of small-scale filamentation instabilities [27] generating X-ray hotspots. Willi *et al* [28] have reported >1.5 keV X-ray hotspots originating from the dense region of plasmas. Herbst *et al* [29] have reported rear side X-ray emission in foil target (12 μm Al) experiments, which clearly showed the presence of these hotspots of few microns in size. We believe that these hotspots are the source for the ionization tracks observed in our case. As the laser intensity

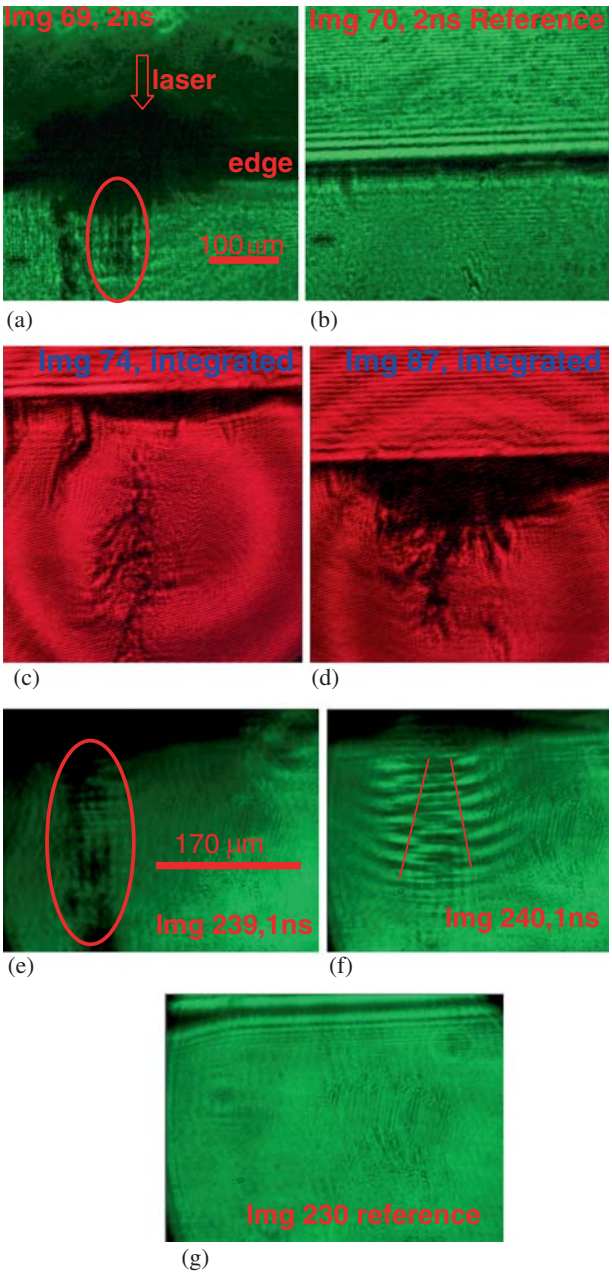

Figure 7. (**a**) Shadowgram showing jet-like structures after a delay of 2 ns; (**b**) a reference shadowgram taken in the absence of plasma (shock); (**c**), (**d**) time-integrated shadowgrams with a He–Ne laser, much after the experiment; (**e**) shadowgram after 1 ns delay; (**f**) shadowgram showing diverging trend in the structure; (**g**) reference shadowgram taken in the absence of plasma (shock).

is varied, the X-ray energy will also change, thus altering their penetration depth in the target material. There is some slight diverging trend in the overall structure of these ionization tracks and only the central tracks are visible after some depth, indicating that the energy of the X-rays on the axis are high compared to others. It can also be seen that the diffraction pattern (generated due to edge diffraction) gets modified at the intersection suggesting X-ray-induced ionization. It is also likely that these ionization tracks may be transient in nature and last for a short time. The presence of ionization tracks in the target region attributed to the X-ray hotspots is not reported in literature. These ionization tracks can be used as signatures to study evolution of the X-ray hotspots using short-duration optical probing techniques.

4. Conclusions

The temporal profile of the propagating shock wave in a transparent medium (soda lime glass) was obtained by using chirped pulse as well as snap-shot shadowgraphy techniques. These are much simpler techniques compared to other techniques like VISAR etc., provided, one has a synchronized pulse as the probe. By optimizing the chirp parameters of the probe beam, one can obtain either the complete temporal profile with lower time resolution, or a part of the profile in a small time window with better temporal resolution. The scaling of the shock velocity with laser intensity has been obtained as $I^{0.38}$. The present optical shadowgraphy experiments have also revealed the presence of jet-like ionization channels that appeared in the target material which had been attributed to the X-ray hotspots generated due to small-scale filamentation instabilities. In addition, the electrical break-down between the charged plasma and the target contributes a permanent tree-like structure in the medium.

Acknowledgements

The authors would like to acknowledge the help of A P Kulkarni, S Jain, D Daiya and A K Sharma on the laser side, and M S Ansari, C P Navathe, N Sreedhar, R Singh and other electronics team members for the electronics support during the experiments. The prompt help from R P Kushwaha in making the target rotator is greatly acknowledged. The enthusiastic participation of M Goswami, M. Tech Project Trainee from School of Physics, DAVV, Indore is greatly acknowledged.

References

[1] S X Hu *et al*, *Phys. Rev. E* **89**, 0631041 (2014)
[2] F H Shu, The physics of astrophysics, in: *Gas dynamics* (University Science Books, Sausalito, CA, 1992) Vol. II, p. 493
[3] T J Ahrens, in: *Methods of experimental physics* edited by C G Sammis and T L Henyey (Academic Press, Orlando, FL, 1987) Vol. 24, Part A, p. 185
[4] R Jeanloz *et al*, *P.N.A.S.* **104**, 9172 (2007)
[5] N C Holmes *et al*, *Phys. Rev. B* **52**, 15835 (1995)
[6] W J Nellis *et al*, *J. Chem. Phys.* **79**, 1480 (1983)
[7] D Batani *et al*, *Phys. Rev. B* **61**, 9287 (2000)
[8] R Cauble *et al*, *Phys. Rev. Lett.* **70**, 2102 (1993)
[9] W Grigsby *et al*, *J. Appl. Phys.* **105**, 0935231 (2009)
[10] L R Henderson, *Handbook of shock waves* (Academic Press, San Diego, CA, 2001) Vol. 1, Chap. 2
[11] R G Trainor and Y T Lee, *Phys. Fluids* **25**, 1898 (1982)
[12] F Cottet *et al*, *Phys. Rev. Lett.* **52**, 1884 (1984)
[13] T R Boehly *et al*, *Phys. Plasmas* **13**, 0563031 (2006)
[14] Y B S R Prasad *et al*, *Rev. Sci. Instrum.* **77**, 093106 (2006)
[15] R R Ecault *et al*, *J. Phys. D* **46**, 235501 (2013)
[16] C P J Barty *et al*, *Opt. Lett.* **21**, 668 (1996)
[17] A S Joshi *et al*, *Fusion Engg. Design* **44**, 067 (1999)
[18] A K Sharma *et al*, *Opt. Commun.* **252**, 369 (2005)
[19] D E Grady and L C Chhabildas, *Shock wave properties of soda lime glass*, Report No: SAND-96-2571C, Sandia National Labs., Albuquerque, NM, United States (1996)
[20] R Ramis *et al*, *Comp. Phys. Commun.* **49**, 475 (1988)
[21] T Kobayashi *et al*, *J. Appl. Phys.* **83**, 1711 (1998)
[22] R Fedosejevs *et al*, *J. Appl. Phys.* **52**, 4186 (1981)
[23] R F Benjamin *et al*, *Phys. Rev. Lett.* **42**, 890 (1979)
[24] J L Borowitz *et al*, *J. Phys. D: Appl. Phys.* **20**, 210 (1987)
[25] D von der Linde and H Schuler, *J. Opt. Soc. Am. B* **13**, 216 (1996)
[26] L Gremillet *et al*, *Phys. Rev. Lett.* **83**, 5015 (1999)
[27] Z Lin *et al*, *High Power Laser Sci. Engg.* **1**, 110 (2013)
[28] O Willi *et al*, *Opt. Commun.* **41**, 110 (1982)
[29] M J Herbst *et al*, *Phys. Rev. Lett.* **46**, 328 (1981)